RAA 2019 Vol. **19** No. **5**, 73(10pp) doi: 10.1088/1674–4527/19/5/73

http://www.raa-journal.org *http://iopscience.iop.org/raa*

***R**esearch in*
***A**stronomy and*
***A**strophysics*

One large glitch in PSR B1737−30 detected with the TMRT

Jie Liu[1,4,5], Zhen Yan[1,6], Jian-Ping Yuan[2,6], Ru-Shuang Zhao[1,5], Zhi-Peng Huang[1,4], Xin-Ji Wu[3], Na Wang[2,6] and Zhi-Qiang Shen[1,4,6]

[1] Shanghai Astronomical Observatory, Chinese Academy of Sciences, Shanghai 200030, China; *yanzhen@shao.ac.cn*
[2] Xinjiang Astronomical Observatory, Chinese Academy of Sciences, Urumqi 830011, China
[3] School of Physics, Peking University, Beijing 100871, China
[4] School of Physical Science and Technology, ShanghaiTech University, Shanghai 201210, China
[5] University of Chinese Academy of Sciences, Beijing 100049, China
[6] Key Laboratory of Radio Astronomy, Chinese Academy of Sciences, Nanjing 210008, China

Received 2018 September 30; accepted 2018 November 25

Abstract One large glitch was detected in PSR B1737−30 using data spanning from MJD 57999 to 58406 obtained with the newly built Shanghai Tian Ma Radio Telescope (TMRT). The glitch took place at the time around MJD 58232.4 when the pulsar underwent an increase in the rotation frequency of $\Delta\nu$ about 1.38×10^{-6} Hz, corresponding to a fractional step change of $\Delta\nu/\nu \sim 8.39 \times 10^{-7}$. Post-glitch ν gradually decreased to the pre-glitch value. The frequency derivative was observed to undergo a step change of about $-9\times10^{-16}\,\mathrm{s}^{-2}$. Since July 1987, there have been 36 glitches already reported in PSR B1737−30 including this one. According to our analysis, the glitch size distribution is well described by a power law with an index of 1.13. The distribution of the interval between two adjacent glitches (waiting time ΔT) follows a Poisson probability density function. For PSR B1737−30, the interval is prone to be long after a large glitch. However, no correlation is found between glitch size and the interval since the previous glitch.

Key words: stars: neutron — pulsars: general — pulsars: individual: B1737−30

1 INTRODUCTION

In general, pulsars rotate with high stability, making it possible to predict the time of arrival (TOA) of each pulse over a long time span. However, two kinds of timing irregularities have been detected in pulsar rotation evolutions: timing noise and glitches. Timing noise is a kind of long-term stochastic fluctuation in residuals. It is related to the pulsar characteristic age $\tau_c = P/(2\dot{P})$ and the spin-down rate $|\dot{\nu}|$ (Hobbs et al. 2010). By comparison, a glitch is a sudden change in the rotation frequency.

Since the first glitch was detected in Vela pulsar (B0833−45) (Radhakrishnan & Manchester 1969; Reichley & Downs 1969), there have been about 520 glitches detected in 180 pulsars (Manchester 2018). Almost all frequency jumps ($\Delta\nu$) caused by glitches are positive except for two negative cases in PSRs J1522−5735 (Pletsch et al. 2013) and J2301+5852 (Archibald et al. 2013). The distribution of $\Delta\nu$ ranges widely from 10^{-11} to 10^{-4} Hz (Espinoza et al. 2011; Fuentes et al. 2017). The smallest glitch was detected in PSR J0631−0200 with a $\Delta\nu/\nu$ of about 2.5×10^{-12} (McKee et al. 2016), and the largest glitch was observed in PSR J1718−3718 with a $\Delta\nu/\nu$ of about 3.325×10^{-5} (Manchester & Hobbs 2011). Post-glitch rotation frequency relaxes back towards the pre-glitch value in most cases. Exponential processes are observed in the relaxation process for some glitches. The timescale of relaxation evidently differs from one glitch to another, ranging from minutes to years (Lyne et al. 1996; Dodson et al. 2007).

Half a century has passed since the first pulsar glitch was detected, but glitch events are still not well understood. The vortex model (Anderson & Itoh 1975; Alpar et al. 1984; Haskell & Melatos 2015) is commonly used to explain the internal mechanism of a glitch. In this scenario, neutrons in pulsar interiors are assumed to form a superfluid (Baym et al. 1969). Vortices are pinned to nuclei in the solid crusts or cores of pulsars and are limited

in their movement outward due to the interaction with ions in the neutron star, so the superfluid cannot loose vorticity to spin down and rotates faster than the crust. Once the Magnus force frees vortices, the angular momentum is transferred rapidly from superfluid to crust, initiating a rise in crust rotation. Soon after the glitch, the vortices are repinned to other regions, causing the relaxation of rotation frequency towards the initial value. There is another kind of timing irregularity named a slow glitch, where ν gradually increases after the glitch and the $|\dot{\nu}|$ undergoes a quick decrease accompanied by an exponential recovery (Zou et al. 2004; Shabanova 2005). It is predicted that the temperature fluctuation of the neutron star will cause a gradual increase in rotation frequency (Greenstein 1979). A slow glitch happens if the local temperature in the inner crust increases suddenly (Link & Epstein 1996). The decrease in $|\dot{\nu}|$ may be a response to the decrease in braking torque (Shabanova 2005).

PSR B1737−30 was detected in the high-radio-frequency survey at Jodrell Bank (Clifton & Lyne 1986) in 1986. Its rotation period is 0.607 s and the period derivative is about 4.66×10^{-13} s s^{-1} (Yuan et al. 2010), suggesting a young characteristic age $\tau_{\rm c}$ of 20.6 kyr. The parameters of PSR B1737−30 are listed in Table 1. PSR B1737−30 exhibits frequent glitch events with 35 glitches reported during MJD 46991 (1987 July 15) and 57499 (2016 April 21). The timing properties of this pulsar were also monitored by the Shanghai Tian Ma Radio Telescope (TMRT) which is a newly built radio telescope with a diameter of 65 m. In this paper, we report one large glitch detected by the TMRT. The structure of this paper is organized as follows. Observations together with data analysis are described in Section 2. Detailed results are shown in Section 3. The discussion and a short conclusion are presented in Section 4 and Section 5 respectively.

2 OBSERVATIONS AND ANALYSIS

Timing observations of PSR B1737−30 were carried out at the wavelength of 13 cm with the TMRT between MJD 57999 (2017 September 3) and 58406 (2018 October 15), using the S-band cryogenically cooled, dual-polarization receiver. The effective frequency coverage of the receiver ranges from 2.2 to 2.3 GHz (Yan et al. 2018). The full bandwidth is divided into channels with a typical width of 1 MHz for convenience in removing the dispersion effect and radio frequency interference (RFI). Data sampling and recording are accomplished using the digital backend system (DIBAS) with a time resolution of 40.96 μs (Yan et al. 2017). The incoherent dedispersion on-line folding observation mode was used in the timing observations with subintegration time of 30 s (Yan et al. 2015). The folding parameters are obtained from the Australia Telescope National Facility (ATNF) Pulsar Catalogue (Manchester et al. 2005)[1]. The observation data are written out as 8-bit PSRFITS files. Each period is divided into 1024 phase bins. The durations of observations were mostly from 10 to 20 min, depending on observation conditions (e.g., weather, RFI, etc.).

In the pulsar timing observations, the time was kept with a local hydrogen atomic clock corrected to GPS. Data reduction and analysis were performed using the PSRCHIVE (Hotan et al. 2004) and TEMPO2 (Hobbs 2012) programs. Data from all channels and subintegrations were scrunched together to get the mean pulse profile for each single observation. Pre- and post-glitch pulse profiles were integrated separately. The integrated normalized pulse profiles are shown in Figure 1. There is no obvious difference between the widths of pulse profiles before and after the glitch (Fig. 2). Local pulse TOAs were generated through the cross-correlation of observed pulse profiles with a high signal to noise ratio (SNR) pulse profile (template). They were converted to TOAs at the solar system barycenter with the Jet Propulsion Laboratory's DE405 ephemeris (Standish 1998). TOA errors are mostly in the range of 20–50 μs. The pulse phase ϕ at the solar system barycenter given by the model is a Taylor series which can be described as a function of time t as

$$\phi(t)=\phi_0+\nu(t-t_0)+\frac{1}{2}\dot{\nu}(t-t_0)^2+\frac{1}{6}\ddot{\nu}(t-t_0)^3+\cdots, \quad (1)$$

where ϕ_0, ν, $\dot{\nu}$ and $\ddot{\nu}$ are the phase at t_0, and the rotation frequency with its first and second time-derivatives, respectively.

Post-glitch frequency typically relaxes back towards its pre-glitch value in the form of

$$\nu(t)=\nu_0(t)+\Delta\nu_{\rm p}+\Delta\dot{\nu}_{\rm p}t+\Delta\nu_{\rm d}e^{-t/\tau_{\rm d}}, \quad (2)$$

$$\dot{\nu}(t)=\dot{\nu}_0(t)+\Delta\dot{\nu}_{\rm p}+\Delta\dot{\nu}_{\rm d}e^{-t/\tau_{\rm d}}, \quad (3)$$

where $\Delta\nu_{\rm p}$, $\Delta\dot{\nu}_{\rm p}$, $\tau_{\rm d}$ and $\Delta\nu_{\rm d}$ are permanent changes in ν and $\dot{\nu}$ relative to pre-glitch values, time constant and amplitude of exponential decay, respectively. The total frequency increment caused by a glitch is

$$\Delta\nu=\Delta\nu_{\rm p}+\Delta\nu_{\rm d}. \quad (4)$$

The degree of recovery can be described by the parameter Q

$$Q=\Delta\nu_{\rm d}/\Delta\nu. \quad (5)$$

[1] *http://www.atnf.csiro.au/research/pulsar/psrcat/*

Table 1 Parameters of PSR B1737−30

Name		RA	DEC	P	$\dot{P}$	τ_c	DM	S_{1400}
B1950	J2000	(h m s)	(d m s)	(s)	(10^{-13} s s^{-1})	(10^3 yr)	(pc cm^{-3})	(mJy)
B1737−30	J1740−3015	17:40:33.82	−30:15:43.5	0.60688662425	4.66124	20.6	151.96	8.9

Notes: All these parameters are referenced from the ATNF Pulsar Database (*http://www.atnf.csiro.au/research/pulsar/psrcat/*). S_{1400} is the flux density at 1.4 GHz.

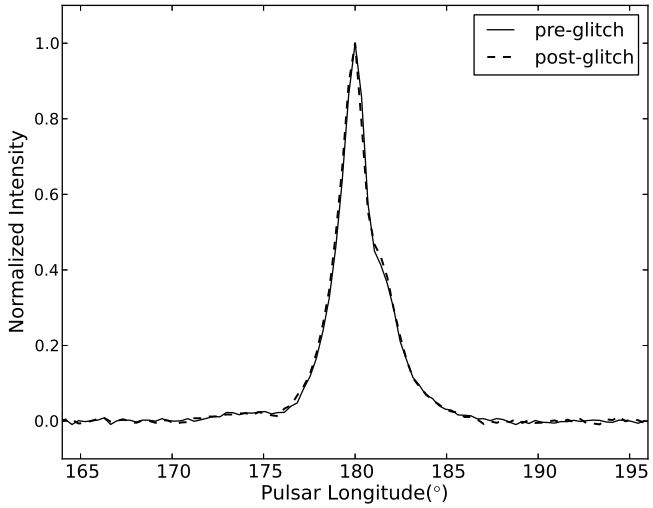

Fig. 1 The integrated normalized pulse profiles of pre- and post-glitch.

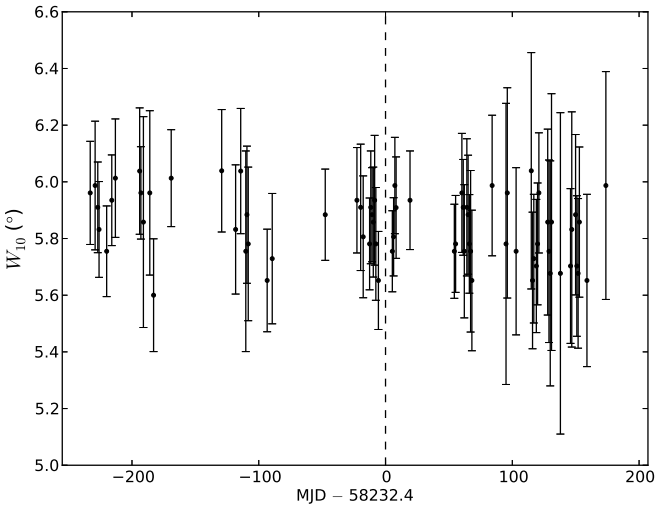

Fig. 2 Distribution of W_{10} in units of degree. The *dashed vertical line* implies the epoch of the glitch.

The results for PSR B1737−30 were obtained using observation data ranging from MJD 57999 to 58406. Timing residuals are the difference between barycentric TOAs and the predicted TOAs, which are randomly distributed around zero if the rotation of the pulsar is described well by the simple spin-down model. Once a glitch happens, the rotation suddenly speeds up (or down), causing the TOAs of pulses to be earlier (or later) than what were predicted by the model. So, the timing residuals will obviously decrease towards a negative (or positive) value. Timing residuals for PSR B1737−30 in the left panel of Figure 3 show an obvious downward trend after MJD

58232.4 (2018 April 24), suggesting a large glitch at that time. In order to confirm whether this glitch event was triggered by an improperly corrected jump and drift of clocks or not, we did further timing analysis of the millisecond pulsar B1937+21 (Backer et al. 1982), which was also monitored at TMRT with the same setups. The timing residuals are displayed in the right panel of Figure 3. As no obvious change was found in the residuals of PSR B1937+21 around MJD 58232.4, the distinct change in the residuals of PSR B1737−30 was caused by the glitch. Since the data interval around the glitch is about 11 d, the final glitch epoch was estimated in two steps. Firstly, it was estimated as the midpoint of the interval. Then, we fitted all the glitch parameters using TEMPO2 while changing the glitch epoch. The final epoch value was selected when chi-square (χ^2) became minimum. The error of glitch epoch was taken as the region of epochs corresponding to $\Delta\chi^2 \leq 1$ from the minimum. Pre- and post-glitch frequency parameters were revealed by fitting ν, $\dot{\nu}$ and $\ddot{\nu}$ with data before and after the glitch separately. In order to investigate the evolution of ν and $\dot{\nu}$ around the glitch, we calculated frequency residuals at various epochs. They were obtained by fitting Equation (1) (omitting the $\ddot{\nu}$ term) over a series of overlapping data sections (Table 2). The timescales of data sections range from 13 to 80 d. The epoch of each fit was set to be the middle date of the data section.

3 RESULTS

The timing solutions of PSR B1737−30 around MJD 58232.4 are listed in Table 3 together with glitch parameters. The glitch parameters were obtained by fitting Equations (2) and (3) with TEMPO2. Timing residuals relative to the pre-glitch rotation model are displayed in Figure 3 (left panel). The residuals between MJD 57999 and 58227 are randomly distributed around zero, implying that the model fits well. After the occurrence of the glitch, residuals continuously decreased towards a negative value. The root mean square (RMS) residual is 201.27 µs after subtracting the fitted glitch model, which corresponds to $\sim$ 0.001 turns. The evolution behaviors of ν and $\dot{\nu}$ are shown in Figure 4. The variations in ν with pre-glitch model subtracted are plotted in panel (a). It shows a remarkable increment of about 1.38×10^{-6} Hz, corresponding to $\Delta\nu/\nu \sim 8.39\times10^{-7}$. This increment is also demonstrated by pre- and post-glitch ν values listed in Table 3. After subtraction of the mean values separately for pre- and post-glitch ν, it is obvious in panel (b) that ν exponentially decayed towards its initial value after the glitch. The time constant of the exponential decay $\tau_{\rm d}$ was fitted to be 71 d. The amplitude of $\Delta\nu_{\rm d}$ is about 9.5×10^{-9} Hz, possibly implying a small value of recovery index Q. Panel (c) shows that the spin-down rate $|\dot{\nu}|$ underwent an increase of about 9×10^{-16} s^{-2}, corresponding to $\Delta\dot{\nu}/\dot{\nu} \sim 7.1\times10^{-4}$. It decreased back towards its initial value after the glitch. There was an increase in $\ddot{\nu}$ (see Table 3), which was caused by the post-glitch recovery.

4 DISCUSSION

As of April 2018, PSR B1737−30 has been observed to exhibit 36 glitches, including this one. Information about glitch epoch, glitch interval, $\Delta\nu/\nu$ and associated reference for all the 36 glitches is listed in Table 4. The fractional increase of $\Delta\nu/\nu$ widely ranges from 7×10^{-10} to $\sim 2.66 \times 10^{-6}$. The $\Delta\nu/\nu$ of the glitch detected by the TMRT is about 8.39×10^{-7}, making it the 4th largest glitch known in this pulsar.

The parameter $A_{\rm g}$ is defined as the mean fractional frequency variation per year caused by glitches

$$A_{\rm g} = \frac{1}{T_{\rm g}} \sum \frac{\Delta\nu}{\nu}, \tag{6}$$

where $\sum(\Delta\nu/\nu)$ is the sum of fractional increments in ν of all glitches during the interval $T_{\rm g}$ (McKenna & Lyne 1990). $A_{\rm g}$ depends not only on how frequently the glitches occurred, but also on the size of the glitches. This makes it a good indicator of glitch events over a long timescale, as it is mainly dominated by large glitches and is insensitive to small glitches which are sometimes difficult to distinguish from timing noise. The glitch activity parameter $A_{\rm g}$ of PSR B1737−30 is about 3.17×10^{-7} yr^{-1}.

Besides PSR B1737−30, there are other pulsars with various glitches reported. The parameters of eight pulsars with at least 10 glitches recorded are provided in Table 5. The glitch size $\Delta\nu/\nu$, time span and $\tau_{\rm c}$ are referenced from the ATNF Pulsar Database. The parameter $T_{\rm g}$ is calculated as the length of the time span in years. This table is listed in sequence of $\tau_{\rm c}$. From the last two columns, $A_{\rm g}$ generally decreases when $\tau_{\rm c}$ increases for pulsars with $\tau_{\rm c} \geq 4$ kyr, but the Crab pulsar (B0531+21) (Staelin & Reifenstein 1968) is an exception. Most of the 25 glitches detected in this pulsar are small or medium-sized glitches. Only two relatively large glitches were measured with $\Delta\nu/\nu$ about 2.14×10^{-7} and 4.8×10^{-7} on MJD $\sim$ 53067.1 and 58064.6, respectively. There is a possible explanation for the relatively weak glitch events of the Crab. Very young pulsars with $\tau_{\rm c}$ smaller than 2 kyr have a higher temperature which reduces the effect of the pinning force and makes it easier for superfluid vortices to move outward. As

Table 2 Timing Solutions of Data Sections

Data section (MJD)	Epoch (MJD)	ν (s^{-1})	$\dot{\nu}$ ($10^{-12}\,s^{-2}$)	Number of TOAs
57999–58012	58006	1.6474050385(1)	−1.2639(7)	5
58012–58039	58025	1.6474050387(1)	−1.2647(4)	5
58038–58063	58050	1.64740503873(4)	−1.2638(1)	6
58063–58124	58113	1.64740503875(5)	−1.2641(8)	7
58114–58185	58132	1.64740503876(6)	−1.2638(6)	8
58139–58220	58199	1.64740503883(4)	−1.2641(3)	7
58184–58227	58225	1.6474050387(1)	−1.2649(7)	10
58237–58252	58244	1.6474064190(2)	−1.2668(8)	5
58286–58301	58293	1.6474064104(1)	−1.2643(9)	10
58316–58353	58335	1.6474064051(1)	−1.2649(2)	10
58347–58370	58350	1.6474064033(2)	−1.2653(7)	11
58360–58385	58373	1.6474064013(1)	−1.2655(6)	11
58363–58406	58395	1.6474063999(3)	−1.2652(1)	10

Table 3 Timing Solutions and Glitch Parameters

Parameter	Pre-glitch	Post-glitch
ν (Hz)	1.64740503872(5)	1.647406475(2)
$\dot{\nu}$ ($10^{-12}\,s^{-2}$)	−1.26397(2)	−1.2678(2)
$\ddot{\nu}$ ($10^{-23}\,s^{-3}$)	−1.6(2)	7.8(7)
Frequency epoch (MJD)	58113	58322
Data span (MJD)	57999–58227	58237–58406
TOA number	32	38
Glitch epoch (MJD)	58232.4(4)	
$\Delta\nu$ (10^{-9} Hz)	1381.7(8)	
$\Delta\nu/\nu$ (10^{-9})	838.7(5)	
$\Delta\dot{\nu}$ ($10^{-16}\,s^{-2}$)	−9.0(4)	
$\Delta\dot{\nu}/\dot{\nu}$ (10^{-3})	0.71(3)	
$\Delta\nu_{\rm d}$ (10^{-9} Hz)	9.5(6)	
$\tau_{\rm d}$ (d)	71(6)	
RMS residual (μs)	201.27	

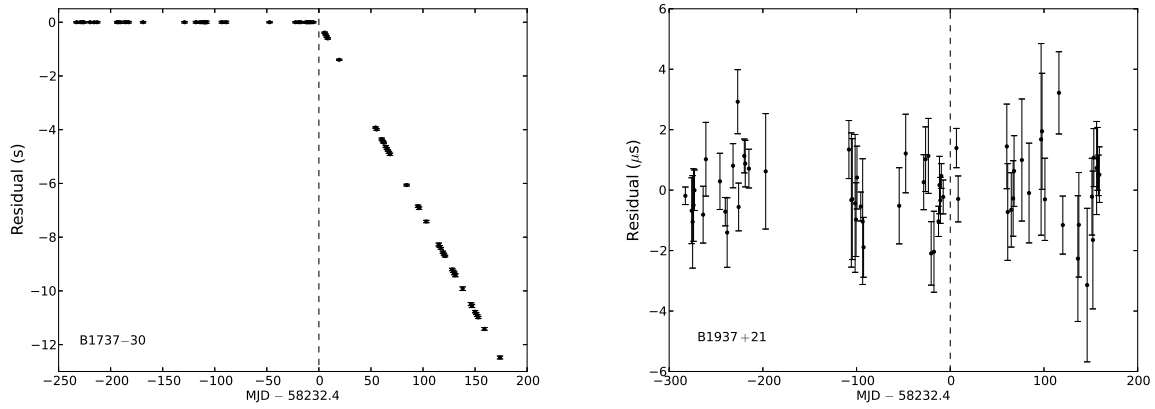

Fig. 3 Timing residuals of PSRs B1737−30 (*left*) and B1937+21 (*right*). The *dashed vertical line* implies the epoch of the glitch.

a result, angular momentum is transferred more smoothly from superfluid to crust, making the glitch size more likely to be small (McKenna & Lyne 1990).

If glitches result from the avalanche process, their sizes follow a power law distribution in the form

$$P(\Delta\nu) = \frac{\Delta\nu^{(1-\alpha)} - \Delta\nu_{\rm min}^{(1-\alpha)}}{\Delta\nu_{\rm max}^{(1-\alpha)} - \Delta\nu_{\rm min}^{(1-\alpha)}} \quad , \qquad (7)$$

Table 4 Information about 36 Glitches in PSR B1737−30

Number	Epoch (T_i) (MJD)	Interval (ΔT_i) (d)	$\Delta\nu/\nu$ (10^{-9})	Reference
1	46991(19)	290(19)	421(4)	[7]
2	47281(2)	51(16)	33(5)	[1]
3	47332(16)	126(16)	7(5)	[1]
4	47458(2)	212.2(20)	30(8)	[1]
5	47670.2(2)	487.8(10)	600.9(6)	[1]
6	48158(1)	33.7(10)	10(1)	[7]
7	48191.69(0)	26.3(20)	659(7)	[7]
8	48218(2)	213.3(20)	48(10)	[2]
9	48431.3(4)	616.2(6)	16(2)	[7]
10	49047.5(5)	191.6(5)	17(1)	[7]
11	49239.07(2)	212.6(4)	169.7(2)	[7]
12	49451.7(4)	92.2(4)	9.5(5)	[4]
13	49543.93(8)	1030.62(8)	3.0(6)	[4]
14	50574.5497(4)	367.0685(4)	439.3(2)	[4]
15	50941.6182(2)	743(21)	1443.0(3)	[3], [4]
16	51685(21)	142(21)	0.7(4)	[5]
17	51827(2)	221(9)	0.9(3)	[7]
18	52048(9)	197(9)	2(3)	[7]
19	52245(2)	21(2)	4(1)	[7]
20	52266.0(2)	81.7(2)	16(1)	[7]
21	52347.66(6)	228.3(30)	152(2)	[6]
22	52576(3)	203.7(30)	0.9(2)	[7]
23	52779.70(4)	79.08(5)	1.7(2)	[7]
24	52858.78(3)	83.7(1)	18.6(3)	[7]
25	52942.5(1)	81.0(1)	20.2(2)	[7]
26	53023.52(0)	450.04(1)	1850.9(3)	[6], [7]
27	53473.56(1)	976.63(1)	0.8(2)	[7]
28	54450.19(1)	245(0)	45.9(3)	[7]
29	54695.19(2)	115.7(1)	3.0(2)	[7]
30	54810.9(1)	117.7(1)	5.2(3)	[7]
31	54928.6(1)	291(14)	2.3(2)	[7]
32	55220(14)	2076(14)	2664.50(15)	[8]
33	57296.5(9)	49.5(11)	1.30(4)	[9]
34	57346.0(6)	153.4(6)	1.94(2)	[10]
35	57499.371(4)	732.0(4)	227.29(3)	[10]
36	58232.4(4)		838.7(5)	this work

Notes: These parameters are referenced from the ATNF Pulsar Database. The glitch interval ΔT_i is defined as: $\Delta T_i = T_{i+1} - T_i$. References: [1] McKenna & Lyne (1990); [2] Shemar & Lyne (1996); [3] Urama (2002); [4] Krawczyk et al. (2003); [5] Janssen & Stappers (2006); [6] Zou et al. (2008); [7] Espinoza et al. (2011); [8] Yu et al. (2013); [9] Jankowski et al. (2015); [10] Jankowski et al. (2016).

Table 5 Glitch Activity Parameters of Eight Frequently Glitching Pulsars

Name	$N_{\rm g}$	$\sum(\Delta\nu/\nu)$ (10^{-9})	Time span (MJD)	$T_{\rm g}$ (yr)	$A_{\rm g}$ (10^{-9} yr^{-1})	$\tau_{\rm c}$ (10^3 yr)
B0531+21	25	977.7(8)	40491.8(3)–58064.555(3)	48.14(0)	20.31(2)	1.26
J0537−6910	23	6614(23)	51285.7(8.6)–53951.2(1.5)	7.26(0)	911(3)	4.93
B0833−45	19	34811(20)	40280(4)–56922(3)	45.59(1)	743.4(4)	11.3
B1338−62	23	11226(6)	47989(21)–55088(16)	19.45(7)	577.2(3)	12.1
B1737−30	36	9765(3)	46991(19)–58232.4(4)	30.80(5)	317.1(1)	20.6
J0631+1036	14	5082.9(6)	50183.5(2)–55702(3)	15.12(1)	336.17(4)	43.6
B1758−23	10	2118(1)	46907(21)–55356(3)	23.15(6)	91.68(6)	58.3
B1822−09	12	242.7(8)	49615(8)–54115.78(4)	12.33(2)	19.68(6)	232

Notes: $N_{\rm g}$ is the number of glitches, and $\sum(\Delta\nu/\nu)$ is the cumulative fractional glitch size for each pulsar. Its error is taken as the variance of errors from each $\Delta\nu/\nu$ for every pulsar. $T_{\rm g}$ equals the corresponding time span in years.

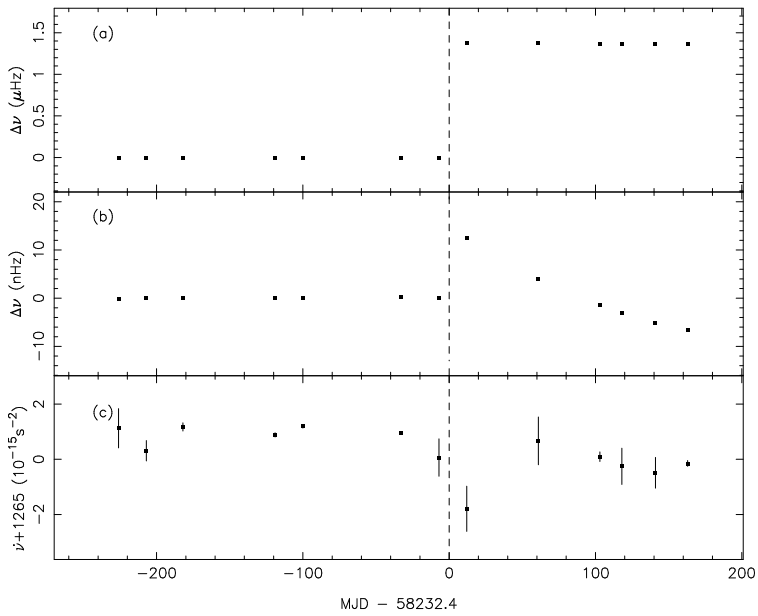

Fig. 4 Frequency variations of PSR B1737−30 relative to pre-glitch solutions. (a) Residuals of $\Delta\nu$ after subtracting the pre-glitch spin-down model; (b) $\Delta\nu$ with mean values removed separately before and after the glitch; (c) The evolution of frequency derivative $\dot{\nu}$ corresponds to an initial value of $|\dot{\nu}|$. The *dashed vertical line* implies the epoch of the glitch.

where α, $\Delta\nu_{\rm max}$ and $\Delta\nu_{\rm min}$ are the power law index and the maximum and minimum frequency jumps, respectively (Melatos et al. 2008). The Kolmogorov-Smirnov (K-S) test statistic D and its associated $P_{\rm K-S}$ are referenced to measure the agreement between data and power law fit. The parameter D is the maximum difference between two data sets, and $P_{\rm K-S}$ means the probability that two sets of data follow the same distribution, equally implying how well the glitch size distribution is described by the power law. For PSR B1737−30, the cumulative glitch size distribution based on glitches before MJD 53190 (2004 July 4) was fitted by a power law function (Melatos et al. 2008). According to their calculation, the $P_{\rm K-S}$ is 0.992 relative to the best fitted α = 1.1, suggesting a good description for cumulative glitch size distribution by the power law. As ten more glitches occurred in PSR B1737−30 after MJD 53190, it is necessary to fit the cumulative glitch size distribution again to test whether it still follows the power law distribution. The power law fit was performed on the 36 glitches as listed in Table 4. The final α value 1.13±0.03 was chosen when the $P_{\rm K-S}$ became maximum. The relative error was estimated as the range corresponding to the $P_{\rm K-S} \geq 0.985$ confidence. The K-S statistic was calculated to be $D = 0.07$ with an associated $P_{\rm K-S} = 0.9996$. This implies that the glitch size distribution for PSR B1737−30 still obeys the power law distribution well, although more glitches with different sizes occurred. Cumulative glitch size distribution of PSR B1737−30 is shown in Figure 5, together with the power law fit described in Equation (7) (dashed curve).

Pulsar glitches are statistically independent if they are caused by an avalanche process. This can be explained by a system in a state of self-organized criticality (SOC). The system is described as a combination of many metastable reservoirs separated from each other by relaxed regions. Accumulated stress in every reservoir is released during one avalanche process. The following avalanche happens randomly and is typically far from the previous one. No interference is found between two adjacent avalanches (Jensen 1998). The interval between two adjacent glitches is defined as waiting time ΔT. Based on the statistical independence of glitches, considering that the system is driven by the nearest local force at a mean rate, the avalanche model predicts that ΔT follows Poisson statistics. So, the distribution of ΔT can be described by a Poisson probability density function as

$$p(\lambda, t) = \lambda^{-1} e^{-t/\lambda} \,, \tag{8}$$

where λ is the mean waiting time. Melatos et al. (2008) fitted the waiting time distribution of PSR B1737−30 over glitches before MJD 53190 with the best fitted $\lambda \sim 242$ d. They proposed that λ is not expected to vary obviously in a range of forty years. We calculated waiting times based on all detected glitches, and got the best fitted λ= 267 d of the Poisson model. This means good consistency with the result calculated in Melatos et al. (2008). The cumulative waiting time distribution and the best model fit

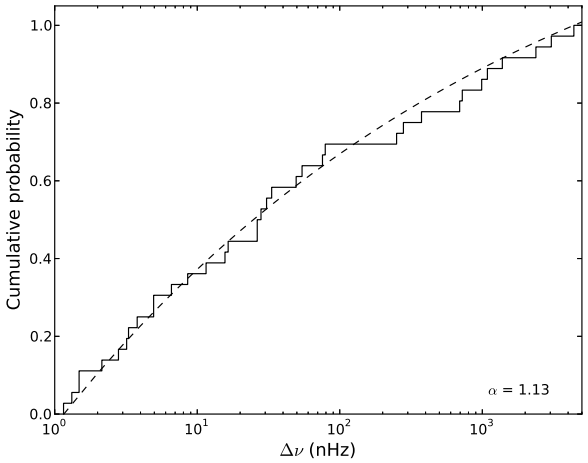

Fig. 5 Cumulative frequency increment distribution of PSR B1737−30 and the power law fit given by Eq. (7) with index α = 1.13 (*dashed curve*).

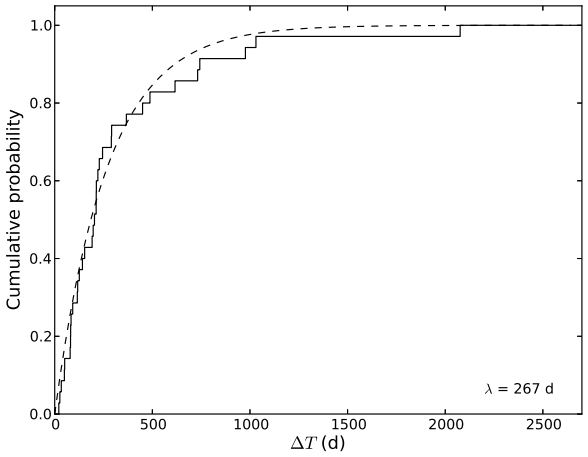

Fig. 6 Cumulative ΔT distribution for PSR B1737−30 corresponding to 35 waiting times and the Poisson model fit in Eq. (8) with λ = 267 d (*dashed curve*). Errors in ΔT are ignored.

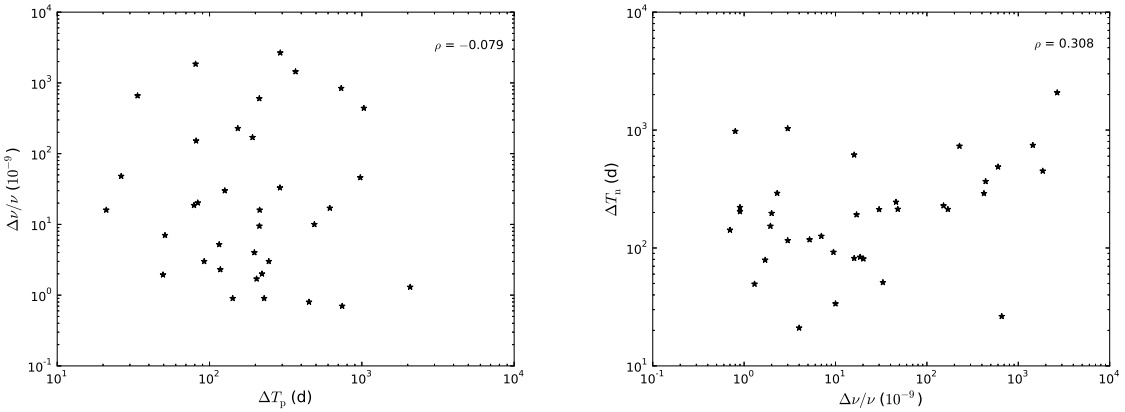

Fig. 7 The relation between $\Delta T_{\rm p}$ and glitch size $\Delta\nu/\nu$ (*left panel*) together with the relation between $\Delta\nu/\nu$ and $\Delta T_{\rm n}$ (*right panel*). Errors in $\Delta\nu/\nu$ and ΔT are ignorable for most points.

(dashed curve) are plotted in Figure 6. The K-S statistic between the data and the Poisson model was calculated to be $D = 0.086$ with the associated $P_{\rm K-S} = 0.999$, implying good agreement between data and model.

There are 36 glitches recorded on PSR B1737−30, making it a good sample to test the correlation between ΔT and glitch size ($\Delta\nu/\nu$). In the left panel of Figure 7, the glitch size is plotted against ΔT since the previous glitch ($\Delta T_{\rm p}$). As data points are so obviously diffuse with the Spearman Rank correlation coefficient $\rho = -0.079$, no correlation is found between them. However, a weak correlation ($\rho = 0.4$) between $\Delta T_{\rm p}$ and glitch sizes of the Crab was proposed, such that large glitches are more likely to occur after long glitch intervals (Shaw et al. 2018). It is necessary to mention that the large glitch at MJD 58064 dominates this correlation of the Crab, and a few small glitches of the Crab happened after long waiting times. This correlation could possibly result from the so called "reservoir effect." In this scenario, the angular momenta are firstly stored then completely released into the crust during a glitch (Haskell & Melatos 2015; Shaw et al. 2018). The ΔT before the next glitch ($\Delta T_{\rm n}$) is plotted against glitch size in the right panel of Figure 7. There is little correlation ($\rho = 0.308$) between these two terms, so that the $\Delta T_{\rm n}$ tends to be long after a large glitch. An apparent correlation ($\rho = 0.931$) was also demonstrated between glitch size and $\Delta T_{\rm n}$ in PSR J0537−6910 (Antonopoulou et al. 2018; Melatos et al. 2018). It is much stronger than that in PSR B1737−30, but is not universally applicable.

5 CONCLUSIONS

We present one large glitch in PSR B1737−30 detected with the TMRT around MJD 58232.4. PSR B1737−30 is the most frequently glitching pulsar known with 36 glitches already detected. The glitch at MJD 58232.4 underwent a frequency increment of $\sim 1.38\times10^{-6}$ Hz, corresponding to a fractional increase of $\Delta\nu/\nu \sim 8.39\times10^{-7}$. The parameter $A_{\rm g}$ is a good indicator of glitch events. For PSR B1737−30, the value of $A_{\rm g}$ is about $3.17\times10^{-7}\,{\rm yr}^{-1}$. Based on the statistics of glitches in eight pulsars with at least 10 glitch events, we find a correlation between $A_{\rm g}$ and characteristic age $\tau_{\rm c}$. For pulsars whose $\tau_{\rm c}$ is greater than 4 kyr, $A_{\rm g}$ generally decreases when $\tau_{\rm c}$ becomes larger. The glitch size distribution of PSR B1737−30 follows a power law distribution with index of 1.13. The distribution of ΔT obeys the Poisson probability density function with best fitted $\lambda = 267$ d. No correlation is found between glitch size and waiting time $\Delta T_{\rm p}$, but the $\Delta T_{\rm n}$ after a large glitch is more likely to be long. Since pulsar glitches differ a lot from one to another even in the same pulsar, a larger glitch sample is valuable for characterizing glitch activities.

Acknowledgements We would like to express our appreciation to Professor R.N. Manchester and anonymous reviewers for their good suggestions on this work. This work was supported in part by the National Natural Science Foundation of China (Grant Nos. U1631122, 11403073 and 11633007), the Strategic Priority Research Program of the Chinese Academy of Sciences (XDB23010200), the Knowledge Innovation Program of the Chinese Academy of Sciences (KJCX1-YW-18) and the National Key R&D Program of China (2018YFA0404602). The hard work of all members of the TMRT team was vital for the high quality observation data used in this paper.

References

Alpar, M. A., Pines, D., Anderson, P. W., & Shaham, J. 1984, ApJ, 276, 325
Anderson, P. W., & Itoh, N. 1975, Nature, 256, 25
Antonopoulou, D., Espinoza, C. M., Kuiper, L., & Andersson, N. 2018, MNRAS, 473, 1644
Archibald, R. F., Kaspi, V. M., Ng, C.-Y., et al. 2013, Nature, 497, 591
Backer, D. C., Kulkarni, S. R., Heiles, C., Davis, M. M., & Goss, W. M. 1982, Nature, 300, 615
Baym, G., Pethick, C., & Pines, D. 1969, Nature, 224, 673
Clifton, T. R., & Lyne, A. G. 1986, Nature, 320, 43
Dodson, R., Lewis, D., & McCulloch, P. 2007, Ap&SS, 308, 585
Espinoza, C. M., Lyne, A. G., Stappers, B. W., & Kramer, M. 2011, MNRAS, 414, 1679
Fuentes, J. R., Espinoza, C. M., Reisenegger, A., et al. 2017, A&A, 608, A131
Greenstein, G. 1979, ApJ, 231, 880
Haskell, B., & Melatos, A. 2015, International Journal of Modern Physics D, 24, 1530008
Hobbs, G. 2012, arXiv:1205.6273
Hobbs, G., Lyne, A. G., & Kramer, M. 2010, MNRAS, 402, 1027
Hotan, A. W., van Straten, W., & Manchester, R. N. 2004, PASA, 21, 302
Jankowski, F., Bailes, M., Barr, E., et al. 2015, The Astronomer's Telegram, 6903
Jankowski, F., Bailes, M., Barr, E., et al. 2016, The Astronomer's Telegram, 9054
Janssen, G. H., & Stappers, B. W. 2006, A&A, 457, 611
Jensen, H. J. 1998, Self-organized Criticality: Emergent Complex Behavior in Physical and Biological Systems, 10 (Cambridge: Cambridge University Press)
Krawczyk, A., Lyne, A. G., Gil, J. A., & Joshi, B. C. 2003, MNRAS, 340, 1087
Link, B., & Epstein, R. I. 1996, ApJ, 457, 844

Lyne, A. G., Kaspi, V. M., Bailes, M., et al. 1996, MNRAS, 281, L14
Manchester, R. 2018, arXiv:1801.04332
Manchester, R. N., & Hobbs, G. 2011, ApJ, 736, L31
Manchester, R. N., Hobbs, G. B., Teoh, A., & Hobbs, M. 2005, AJ, 129, 1993
McKee, J. W., Janssen, G. H., Stappers, B. W., et al. 2016, MNRAS, 461, 2809
McKenna, J., & Lyne, A. G. 1990, Nature, 343, 349
Melatos, A., Howitt, G., & Fulgenzi, W. 2018, ApJ, 863, 196
Melatos, A., Peralta, C., & Wyithe, J. S. B. 2008, ApJ, 672, 1103
Pletsch, H. J., Guillemot, L., Allen, B., et al. 2013, ApJ, 779, L11
Radhakrishnan, V., & Manchester, R. N. 1969, Nature, 222, 228
Reichley, P. E., & Downs, G. S. 1969, Nature, 222, 229
Shabanova, T. V. 2005, MNRAS, 356, 1435
Shaw, B., Lyne, A. G., Stappers, B. W., et al. 2018, MNRAS, 478, 3832
Shemar, S. L., & Lyne, A. G. 1996, MNRAS, 282, 677
Staelin, D. H., & Reifenstein, III, E. C. 1968, Science, 162, 1481
Standish, E. 1998, JPL Planetary and Lunar Ephemerides, DE405/LE405, Memo IOM, 312, F–98–048, *http://ssd.jpl.nasa.gov/iau-comm4/de405iom/de405iom.pdf*
Urama, J. O. 2002, MNRAS, 330, 58
Yan, Z., Shen, Z.-Q., Wu, Y.-J., Zhao, R.-B., & Liu, Q.-H. 2017, in General Assembly and Scientific Symposium of the International Union of Radio Science (URSI GASS), 2017 XXXIInd, IEEE, 1
Yan, Z., Shen, Z.-Q., Wu, X.-J., et al. 2015, ApJ, 814, 5
Yan, Z., Shen, Z.-Q., Manchester, R. N., et al. 2018, ApJ, 856, 55
Yu, M., Manchester, R. N., Hobbs, G., et al. 2013, MNRAS, 429, 688
Yuan, J. P., Wang, N., Manchester, R. N., & Liu, Z. Y. 2010, MNRAS, 404, 289
Zou, W. Z., Wang, N., Manchester, R. N., et al. 2008, MNRAS, 384, 1063
Zou, W. Z., Wang, N., Wang, H. X., et al. 2004, MNRAS, 354, 811